Journal of Asian Earth Sciences 94 (2014) 68–76

Contents lists available at ScienceDirect

Journal of Asian Earth Sciences

journal homepage: www.elsevier.com/locate/jseaes

Deep electrical structure over the igneous arc of the Indo Burman Orogen in Sagaing province, Myanmar from magnetotelluric studies

C.K. Rao *, C. Selvaraj, S.G. Gokarn

Indian Institute of Geomagnetism, Sector-18, New Panvel (W), Navi Mumbai 410218, India

ARTICLE INFO

Article history:
Received 28 August 2013
Received in revised form 1 August 2014
Accepted 9 August 2014
Available online 21 August 2014

Keywords:
Indo Burman Orogen
Magnetotellurics
Indo Myanmar suture

ABSTRACT

Magnetotelluric studies over the igneous arc of the Indo Burman range in the Sagaing province of Myanmar have delineated the high resistivity Indian plate subducting westwards beneath the Burmese block to depths of 30 km and beyond. The thick moderately resistive (20–100 Ω m) layer overlying the subducting Indian plate may be due to the low resistivity sediments. The entire region is covered with prominent sedimentary layer with a conductance varying between 20 and 3000 S showing a general increase from the east to west, suggesting that their thickness increases toward the west. The large unsystematic variations in the conductance are indicative of the widely varying depositional environments and also possible vertical block movements during the course of their deposition. A west dipping low resistivity zone to the east of Burmese block seems to demarcate its eastern limit, suggesting the possibility of a hitherto unknown deep seated fault, which is also supported by the several earthquake foci located over this zone. The nature of the crustal movements over this fault is not immediately apparent. Possibility exists that the Sagaing fault is an en echelon fault and the present feature observed here is a part of this en echelon fault. The possibility of channel flows of the weakened rocks in the deep crust observed in the vicinity of the eastern Himalayan syntaxis may also cause such low resistivity zones.

1. Introduction

Subsequent to the collision between Indian and Eurasian plates leading to the formation of the Himalaya, the Indian plate rotated anti-clockwise, thus causing a compressional tectonic regime over its eastern margin (Curray et al., 1982). These compressive forces along with contribution from the westward drift of the Asian Plate created a long subduction zone and a series of trenches along the present day Indo Burman Orogen, the Andaman Nicobar island chain and the Sumatra arc to the south. Although most of the processes in this region have occurred only in the recent times, during the Cenozoic, the proximity of two major thrust zones, the oblique subduction of the Indian plate beneath the Asian plate, the intense sedimentation coupled with the volcanic activity, have created a complex tectonic and crustal evolutionary setting which have attracted the international scientific attention. Among the several complex tectonic regimes on the eastern fringe of the Indian plate, this sequence of tectonic processes created a long igneous arc to the east of the Indo Burman fold belts. Magnetotelluric (MT) studies have provided useful constraints in mapping the subduction zones elsewhere over the Himalayan Orogen (Gokarn et al., 2002, 2008; Unsworth et al., 2005). Due to the low resistivity of the thermo mechanical flows, these studies are also useful studying the volcanic provinces of the kind observed along the Indo Burman range. With an intention of understanding these processes better, magnetotelluric studies were conducted over an EW profile across the volcanic arc of the Indo Burman subduction zone.

2. Geology and tectonics

The entire Indo Burman range (IBR) and the surroundings show an arcuate tectonic fabric with a general NS strike, east verging on its northern and southern parts. The Major geological features and tectonic elements in this region are shown in Fig. 1 (Modified, after Maurin and Rangin, 2009; Acharya, 2007; Verma et al., 1976; Bender, 1983). Also shown here is the profile used for the MT studies. The NS oriented Sagaing fault is a major lineament running about 200 km east of the IBR and separates the Myanmar central basin from the Shan plateau to the east. The Indo Burman suture located to the west of the IBR is not shown in the figure because it is located under the thick cover of the Irrawaddy sediments which cover the entire survey region and thus this suture has no

* Corresponding author. Address: Indian Institute of Geomagnetism, Plot no. 5, Sector-18, Kalamboli Highway, New Panvel (W), Navi Mumbai 410218, India. Tel.: +91 22 27484134; fax: +91 22 27480762.

E-mail address: ckrao@iigs.iigm.res.in (C.K. Rao).

http://dx.doi.org/10.1016/j.jseaes.2014.08.016
1367-9120/

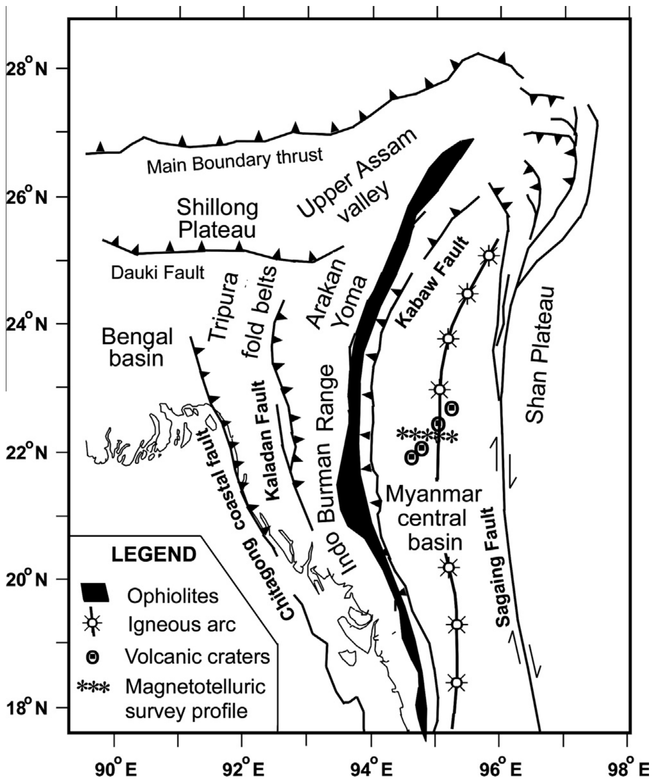

Fig. 1. Geological and tectonic map of the NE India and Northern Myanmar, showing the location of the profile covered for the MT data collection. (Modified after, Maurin and Rangin, 2009; Acharya, 2007; Verma et al., 1976; Bender, 1983).

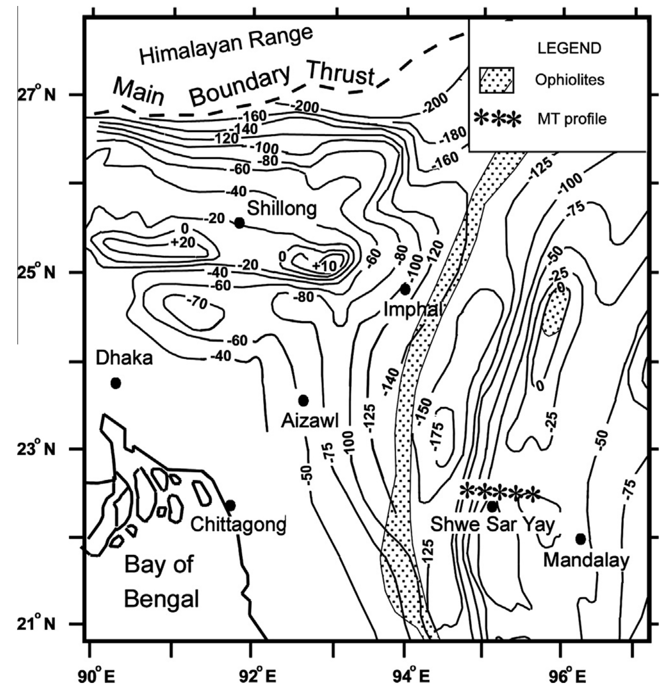

Fig. 2. Bouguer gravity map of the NE India and northern Myanmar (Redrawn from Verma et al., 1976). Also shown is the eastern and western ophiolite belts (Acharya, 2007) and the MT study profile.

surface manifestation. Based on the models developed on the global kinematic processes, Curray et al. (1979) proposed a Burmese plate between these two faults. They also conjectured that the strike slip and the compressional components of the stresses generated by the oblique subduction of the Indian plate might be partitioned, with the strike slip occurring over the Sagaing fault and the subduction along the western margin of the IBR. Based on the seismic and multi beam bathymetric studies over the marine regions of the Andaman arc, Nielsen et al. (2004) observe that the distribution of the stresses over the various faults shows strong spatial variations from purely strike slip to purely compressional, depending upon the orientation of the various local segments.

Based on the results of the global positioning system studies over the eastern Himalayan syntaxis (EHS), Gan et al. (2007) observe "glacier like crustal flows" in the clock-wise direction around EHS from the eastern Himalaya and south eastern China, extending into the Shan plateau region, about 80 km east of the present study region. The surface wave tomographic studies (Yao et al., 2008) have delineated several low velocity layers in the deep crust extending into the upper mantle suggesting that these crustal flows are deep rooted into the crust and upper mantle and are attributed by these authors to weakened crust and upper mantle in this region. The low electric resistivities reported from the MT studies (Denghai et al., 2010) to be discussed later in Sections 5 and 6 corroborate this observation.

The Myanmar central basin is covered by up to 15 km thick Irrawaddy sediments, which get progressively older from Pliocene to the Eocene at deeper strata (Maurin and Rangin, 2009). Two NS trending discrete bands of ophiolitic rocks are delineated as shown in Fig. 2 (Acharya, 2007) first, the western belt (also shown in Fig. 1) located in the Indian states of Nagaland and Manipur, extending into the Andaman islands, accreted during mid-Eocene and the second, the eastern belt, accreted much later during the Cretaceous. The existence of the eastern belt is not obvious because it is poorly exposed, except at the northern end of the magmatic arc (about 150 km north of Shwe Sar Yay in Fig. 2). The western belt is generally believed to be the line of suturing of the subducting Indian plate (Gansser, 1980; Mitchell, 1981; Acharya and Mitra, 1986). However, based on the negative Bouguer gravity anomaly (Fig. 2) associated with the western belt, Acharya (2007) surmises that this belt does not have sufficiently deep roots to justify suturing. The ophiolites over the eastern belt are however associated with a gravity high, indicative of possible deep-rooted high-density ultramafic rocks. Hence, this author suggests that the eastern belt may be the surface expression of the suture.

Detailed gravity studies are not available over the Indo-Burman region. However, the regional Bouguer gravity map of the area obtained by combining the 25 mGal contours over the eastern part of the IBR and the 10 mGal contours on the western part is shown in Fig. 2 (modified after Verma et al., 1976). From the analysis of the Bouguer and isostatic anomaly maps, along with the seismicity records of this region, these authors observe that the region is in general isostatically uncompensated. On the basis of the correlation between the earthquake foci and the isostatic anomalies, they attribute the recent seismicity to the vertical block movements in response to the uncompensated isostacy over IBR and surroundings.

Ni et al. (1989) based on their analysis of some well located earthquake hypocenters observe that the Benioff Wadati zone beneath north Burma shows an eastward dip and slopes by about 50 degrees to the north near EHS and 30 degrees to the south near the Bay of Bengal region. The fault plane solutions for the earthquakes at deeper levels near the subduction zone show the T axes aligned in the direction of the dip. On the basis of this observation these authors suggest that a slab pull mechanism may be playing a major role in the Indian subduction.

We conducted MT studies over a 80 km long EW profile across the volcanic arc in the central Myanmar basin under a sponsored project for characterizing the electrical resistivity structure associated with the igneous activity in the Shwe Sar Yay and surrounding

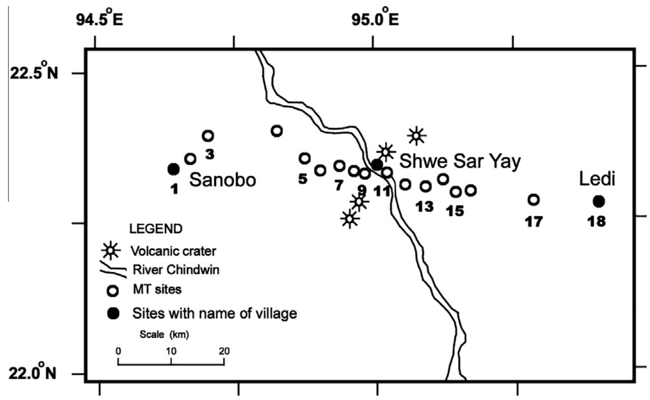

Fig. 3. Location of the sites covered for the MT data collection.

region in the Saggaing province, about 120 km NW of Mandalay. The location map of the sites covered for data collection is shown in Fig. 3. This region is covered by about 10–15 km thick Cenozoic sequences of Irrawaddy sediments and is dotted by several volcanic craters near the Chindwin River.

3. Field survey and data analysis

Broad band MT data (period range of 0.003–10,000 s) were collected at 18 sites over about 80 km long EW profile between Sanobo and Ledi (Fig. 3), with an inter-station spacing of generally about 5–10 km. However due to logistic difficulties, the inter-station spacing was larger than 10 km at some places. Five component MT data were recorded for a period of more than 40 h at each site. Although the regional tectonic features show a predominantly NS strike in the study region, the magmatic exposures as well as the craters of the volcanoes have a NE–SW disposition, thus causing confusion on the possible geoelectric strike direction and the identification of the profile for data collection. In order to resolve this discrepancy in the strike direction, some test sites were covered in the close vicinity of the igneous exposures. These sites indicated a geoelctric strike along NS direction and hence the subsequent sites were selected over an EW profile, (perpendicular to the geoelectric strike). Perhaps some shallow fault striking NE–SW may have influenced the volcanic activity.

The auto and cross power spectra were obtained from the time series using the remote reference techniques of Jones and Jodicke (1984), Jones et al. (1989) which were then used to compute the impedance tensors and tipper. The survey region is located over a top layer of Irrawaddy sediments, the low resistivity of which helps decrease the cultural electromagnetic noise. This fact along with the remoteness of the survey area leading to very low cultural noise, helped an excellent data collection. Some of the unedited response functions (apparent resistivity and phase values) are shown in Fig. 4 along with the error bars corresponding to one standard deviation. Most of the error bars are smaller than the symbol size and hence are not seen in the figure.

The strike directions were determined using tensor decomposition scheme of Groom and Bailey (1989) referred to as GB decomposition in rest part of the paper. As mentioned earlier, due to the low resistivity top layer, most of the distortions caused by the shallow inhomogeneities die down at short distances and thus the shear and twist values which are the measure of such distortions in the GB decomposition scheme are small. Some representative unconstrained results of the GB decomposition of the unedited data at the sites 3 and 13 are shown in Fig. 5 along with those obtained after constraining the shear and twist. The unconstrained strike angles are stable at near zero degrees (suggesting a NS strike) at periods larger than 10 s at the site 3 whereas, the values between 0 and −15 degrees are observed in the period range 0.02–200 s at the site 13. The strike values at other periods are rather noisy with large unsystematic variations. It may be observed from the apparent resistivities and phases at these periods that the response at short periods at site 3 show almost a one dimensional structure at short periods (<10 s). It is thus assumed that the large scatter may be due to the ill-defined strike, as observed in the one dimensional cases. The scatter at the long periods may be due to the poor statistics due to lesser number of stacks. The data at all the other sites showed similar behavior. The GB decomposition was performed at all the other sites on similar lines. The strike angles thus obtained are shown in Fig. 6 along with the constrained values of twist and shear at all the sites. Here the gray bands on the strike plots at individual sites denote a ±10 degree range around the value of zero degrees, corresponding to the north. Most frequencies show a strike angle of NS within the gray band, although at some of the sites a significant scatter is observed in the strike angles. In order to constrain this angle better, the multi-site multi-frequency tensor decomposition (McNeice and Jones, 2001) was used with the impedance error floor set at 3.5% which is equivalent to a phase error of 2 degrees and resistivity error of 7.1%. This procedure yielded a strike angle of −1.9 degrees. In view of this fact, the strike was assumed to be along the NS direction, which is close to the regional strike angle. The geoelectric strike obtained in the MT studies always suffers a 90 degree ambiguity which can be removed using different methods. The induction vectors which are obtained using the magnetic field components help resolve this ambiguity. The strike information available from other geophysical and geological studies is also used for this purpose. The real components of the induction arrows obtained at periods of 1, 10, 100 and 500 s are shown in Fig. 7, such that they point to the low resistivity features in the sub structure. Most of the long arrows (longer than 0.2) point to the east or the west at the sites, to the west of site 8 and also at the sites 16, 17 and 18 to on the eastern flank of the profile, particularly at the periods of 100 and 500 s. The arrows at sites, 9–13 are generally shorter than 0.2, and show rather unsystematic orientation, indicating the possible presence of a low resistivity beneath these sites. The real induction arrows at short periods (1 and 10 s) are shorter than 0.1, indicative of a weak vertical magnetic field, suggestive of a low resistivity top layer throughout the survey profile, caused by the alluvium of the Irrawaddy and Chindwin rivers. The random variation of their directions may be firstly due the large errors in measuring the weak vertical magnetic field and secondly, due to the random variation in the thickness of the alluvial cover. Some contributions from weak three dimensional nature associated with such geological features may also have contributed to the observed random orientation of the induction arrows, as well as of the strike angles in Figs. 6 and 7. On the basis of the foregoing discussion and the NS orientation observed in the regional tectonic fabric, (Fig. 1) as well as the Bouguer gravity contours (Fig. 2) it seems reasonable to assume that the regional strike is along the NS direction. The response functions along this direction were assumed to be the TE mode values and those perpendicular, the TM mode values. The tensor decomposition procedure was repeated with the strike angles fixed along the assumed regional strike angle and the shear and twist fixed at the values obtained at the individual sites and the fully constrained Groom Bailey decomposed apparent resistivities and phases thus obtained are shown in Figs. 8 and 9 in the pseudo section form. Also shown here are the model responses obtained for the geoelectric section shown in Fig. 11.

The GB decomposed response functions were inverted using the 2D inversion program of Rodi and Mackie (2001) using a half space with a resistivity of 100 Ω m as the starting model and a smoothness parameter tau of 5, which was arrived at after attempting the

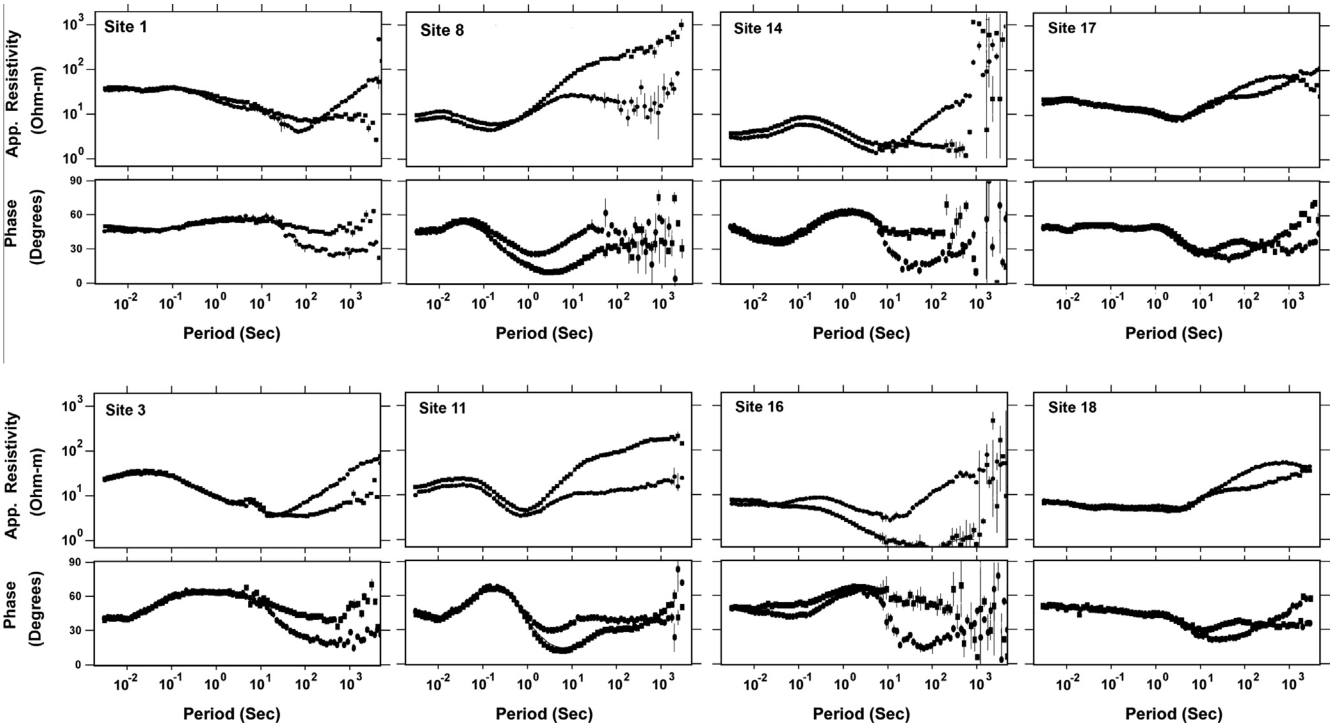

Fig. 4. Unedited apparent resistivity and phase curves at some sites. The error bars are one standard deviation long. Where not shown, the error bars are smaller than the symbol size.

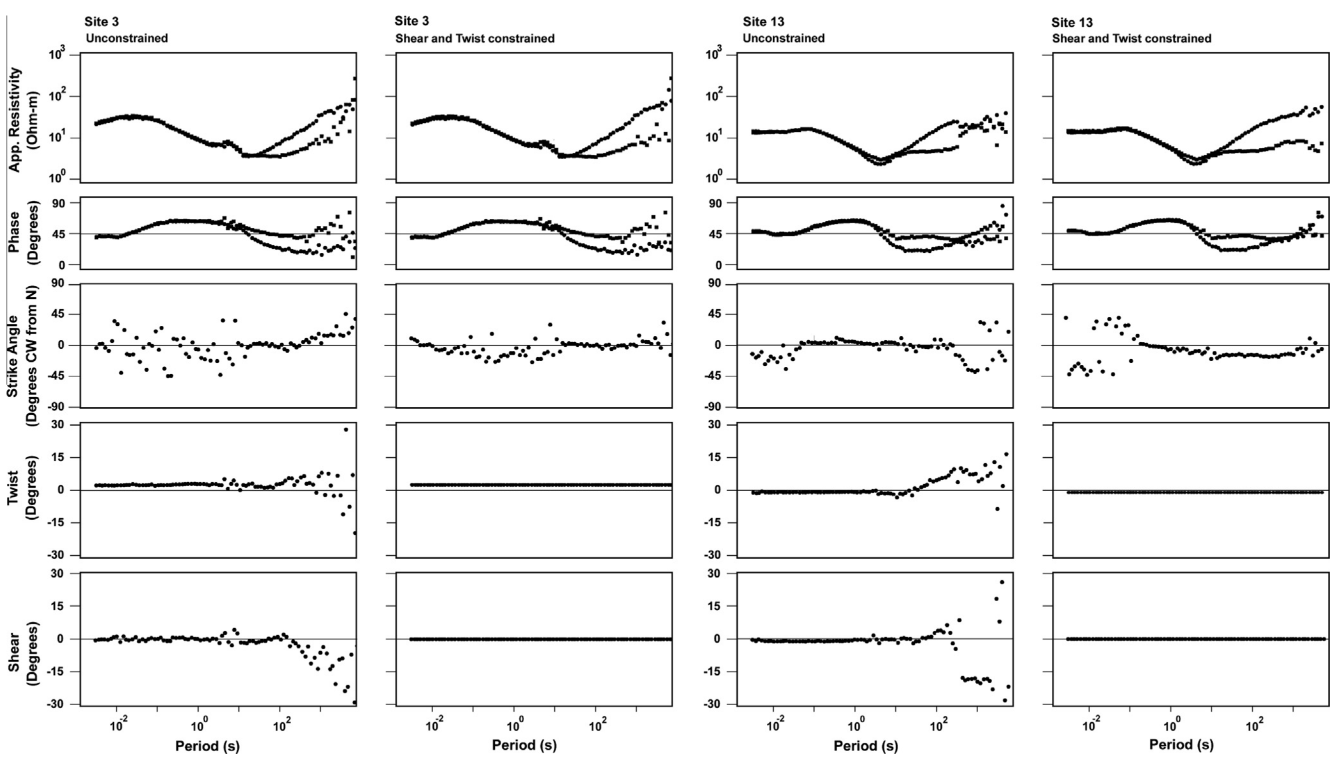

Fig. 5. Results of the unconstrained tensor decomposition and those after constraining the twist and shear at sites 3 and 13. The data are unedited.

inversion with different half-space resistivities of 10, 50, 100, 500 and 1000 Ω m and tau values of 20, 10, 5 and 1. Both the apparent resistivity and phases in the TE and TM modes as well as the tipper data were used for this purpose. The models were also obtained by inverting the TE only and TM only response functions for assessing the possibility of the contribution of the possible weak three dimensionality effects before arriving at the final model presented here. In order to remove the static shift effect, which is essentially the result of the distortions in the induced electric currents by the shallow surface inhomogeneities, the weight of the apparent

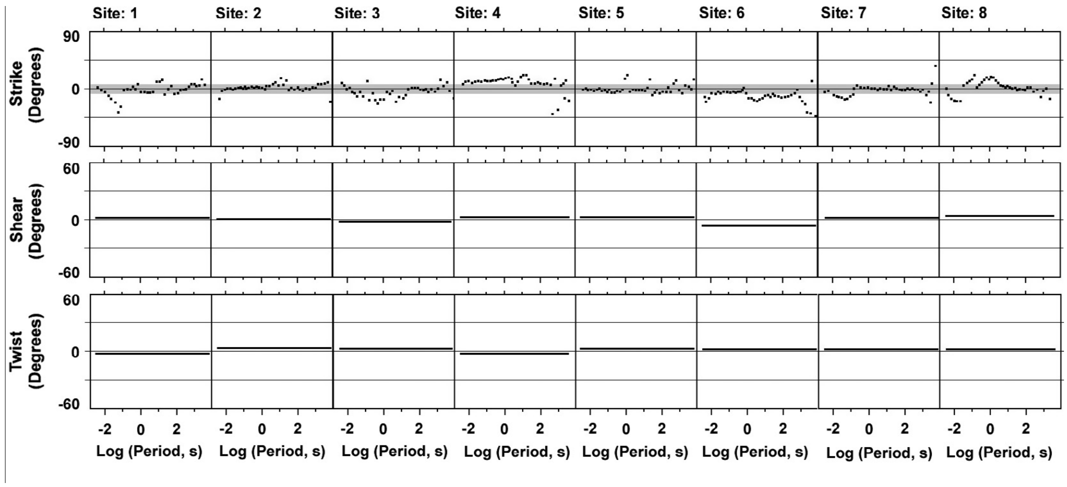

Fig. 6. Strike angles observed after the tensor decomposition at different frequencies at all sites, shown along with the constrained twist and shear values. The gray band on the strike plots represents the ±10 degree range from the NS direction, which is the presumed regional geoelectric strike.

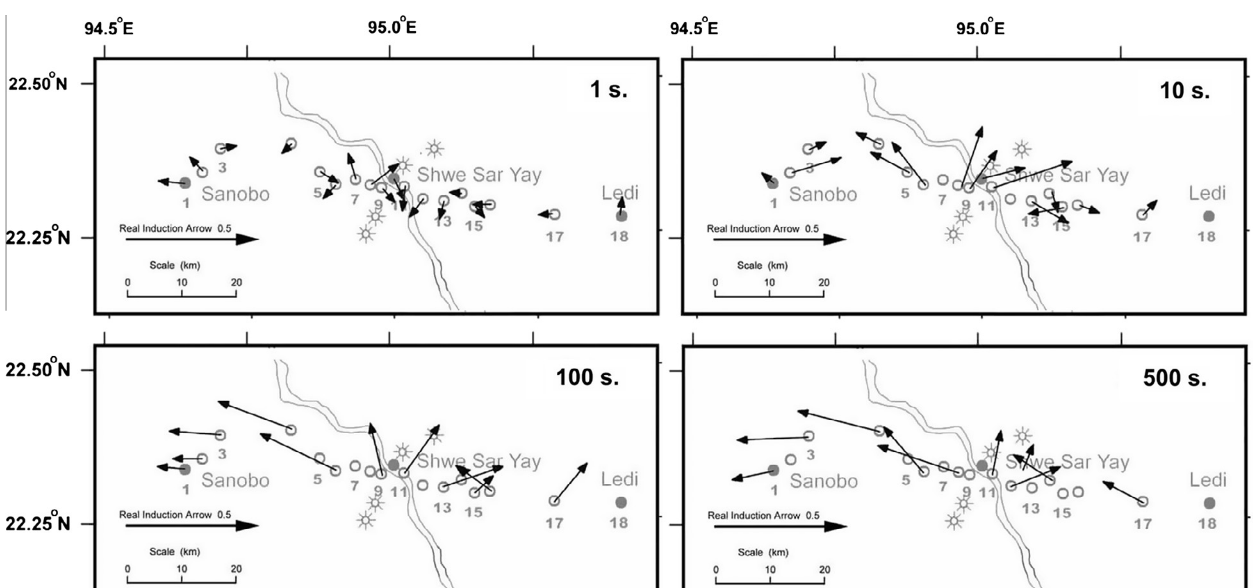

Fig. 7. Real induction vectors at 1, 10, 100 and 500 s at all the sites.

resistivity in the inversion process was decreased by a factor of 100. Thus, the geoelectric structure was strongly determined by the phase data, which are not affected by the static shifts. However the phase data do not contain information on the true resistivity levels and hence the even down-weighted apparent resistivity data are sufficient to constrain the true resistivity levels. In all about

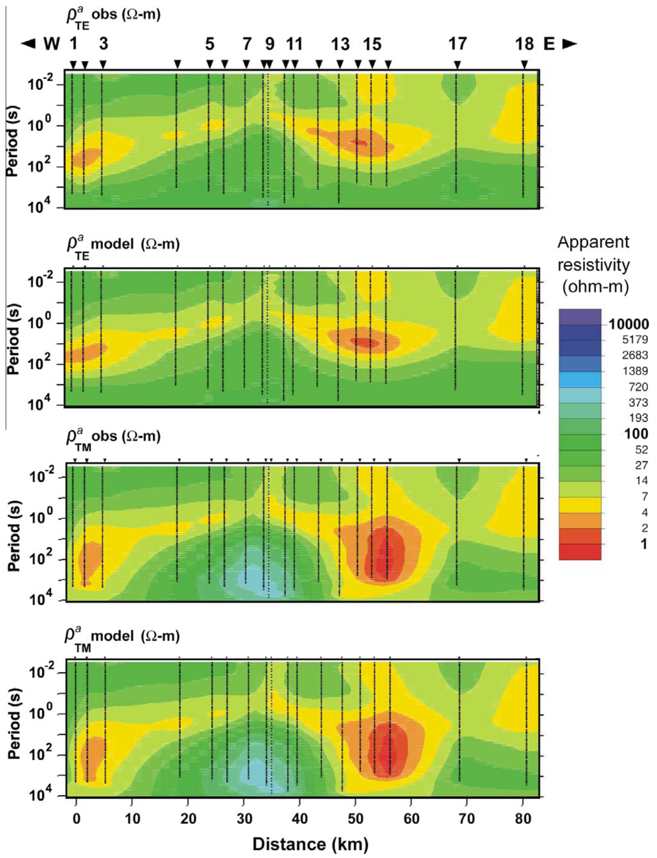

Fig. 8. Observed (Groom Bailey decomposed) and modeled apparent resistivity pseudo sections in the transverse electric and transverse magnetic modes. The dots over the pseudo sections at each site position and period correspond to the observed data points.

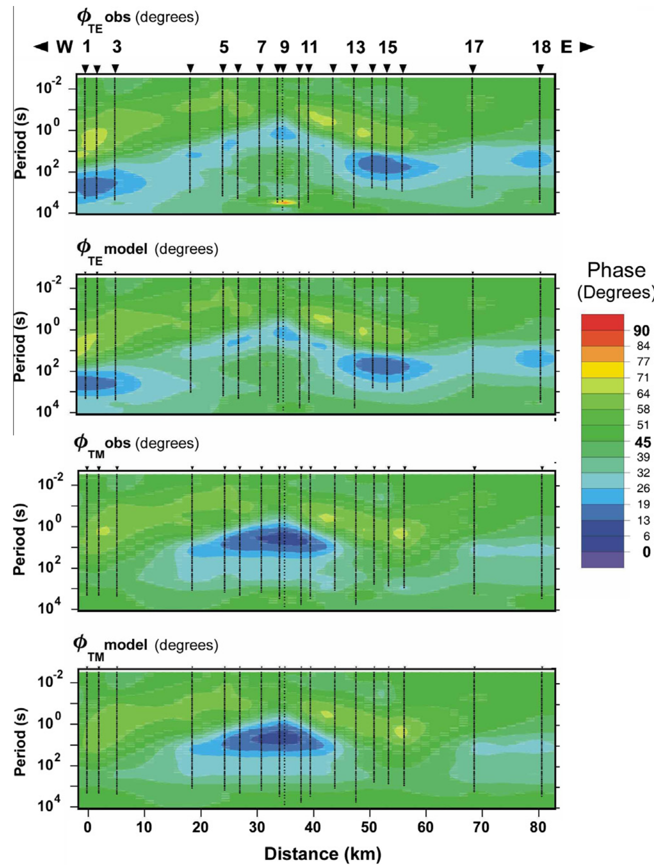

Fig. 9. Observed (Groom Bailey decomposed) and modeled phase pseudo sections in the transverse electric and transverse magnetic modes. The dots over the pseudo sections at each site position and period correspond to the observed data points.

180 iterations were required before stabilizing the inversion process to an RMS misfit of 2.4. The geoelectric model thus obtained is shown in Fig. 11 along with the Bouguer gravity over the MT profile (based on the gravity contours in Fig. 2). The topography along the profile and the location of the volcanic craters are also shown on the top part of this figure. The slanting line marked BW Zone indicates the location of the Benioff Wadati zone reported from the seismic studies (Ni et al., 1989) and the dark circles denote the position of the high accuracy earthquake foci. The pseudo-sections of the apparent resistivity phase and tipper magnitude computed for this model are shown in Figs. 8–10 respectively along with the observed values to facilitate a comparative assessment.

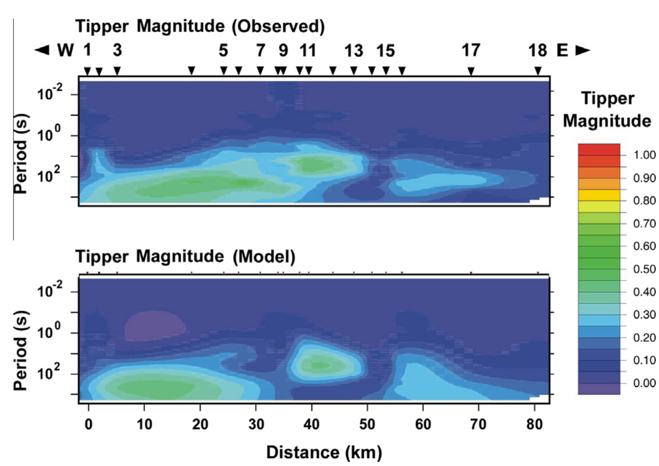

Fig. 10. Observed and modeled tipper magnitudes.

4. Results

For the sake of convenience of discussion here, the major resistivity features in the geoelectric section (Fig. 11) are denoted by alphabets. A moderate to low resistivity top layer, (A–A′–A) with widely varying conductance values in the range of 20 and 3000 S is delineated at all the sites in the survey profile, except between the sites 7–11, in the close vicinity of the volcanic craters. The discontinuity between sites 16 and 17 however may be due the absence of the constraints, caused by the large gap of more than 10 km between these sites. Two high resistivity features (B–B′), merged together at the depths of 15–25 km, are traced underlying the sedimentary layer with resistivity varying from 2000 to 10,000 Ω m, between the sites, 5–13 and 15–17. The low resistivity between the sites 5–13 and 15–17 may be due to the shielding of this high resistivity by the extremely high overburden of conductance (about 1500 S) at the top. In order to ascertain this fact, sensitivity tests were carried out by replacing the high conductance between the two high resistivity bodies with a resistivity similar to those of the two bodies (1500 Ω m). The response functions were unaffected by this change, which provides adequate support to our presumption. Since the shielding of the resistive layers by the overlying high conductance layers is a well-known phenomenon in geoelectromagnetism (Kaufman and Keller, 1981), the results of the sensitivity test are not shown here. Similar shielding

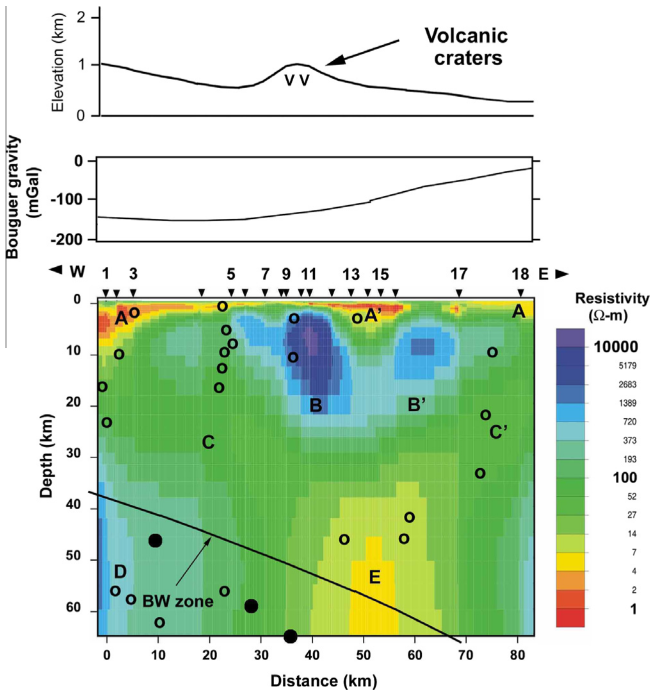

Fig. 11. Geoeletric cross section. The Bouguer gravity (Culled from Fig. 2) along the MT profile is shown on the top part. The major resistivity features are denoted with the alphabets for convenience of reference in the text. " BW zone" denotes the location of the Benioff Wadati zone and the solid circles denote the foci of the earthquakes reported by Ni et al. (1989). The lateral position of the seismic data are matched with the geoelectric section using the position of the volcanic craters shown and is subjective to that extent.

effects are also observed between sites 4 and 5 as well as 16 and 17. Based on this observation, we assume that the resistive features (B–B′) represent a single resistive body, extending continuously over a distance of about 60 km between sites 4 and 17. This feature is surrounded to the east, west as well as at the bottom by the moderate resistivity feature, C–C′ with resistivity of 20–200 Ω m, suggestive of two fault zones to the east and west of B–B′ converging at its base.

A high resistivity body (D) is present at depth of 30 km over the western part of the profile between sites, 1 and 3, probably extending up to site 4. This is indicated in the responses (Figs. 8 and 9) by the increasing apparent resistivity and decreasing phase respectively at periods longer than 300 s at these sites. Further east, a low resistivity feature (E) with a conductance of more than 4000 S is delineated at depth of 30 km and beyond between the sites, 12 and 17. The signatures of this feature are not obvious in the pseudo sections and hence sensitivity studies were carried out to check these signatures in the response functions. In order to test this, the low resistivity zone in the geoelectric section was completely removed by replacing it with resistivity of 150 Ω m observed in its surrounding region. The modeled responses before and after this replacement are shown in Fig. 12 along with the observed data points. Here the apparent resistivity values at long periods (>1000 s) increase and the phases decrease after the removal of the low resistivity body, (E). The larger misfit between the observed and modeled data in apparent resistivity and phase is clearly evident in the long period range after the removal of the feature (E), especially at sites 8 and 11 to the east of the feature (E) as well as the site 13 located on its top part. The phase values at site 13 are higher than 45 degrees, indicating a low resistivity at the corresponding depths. In MT responses, phase increases to

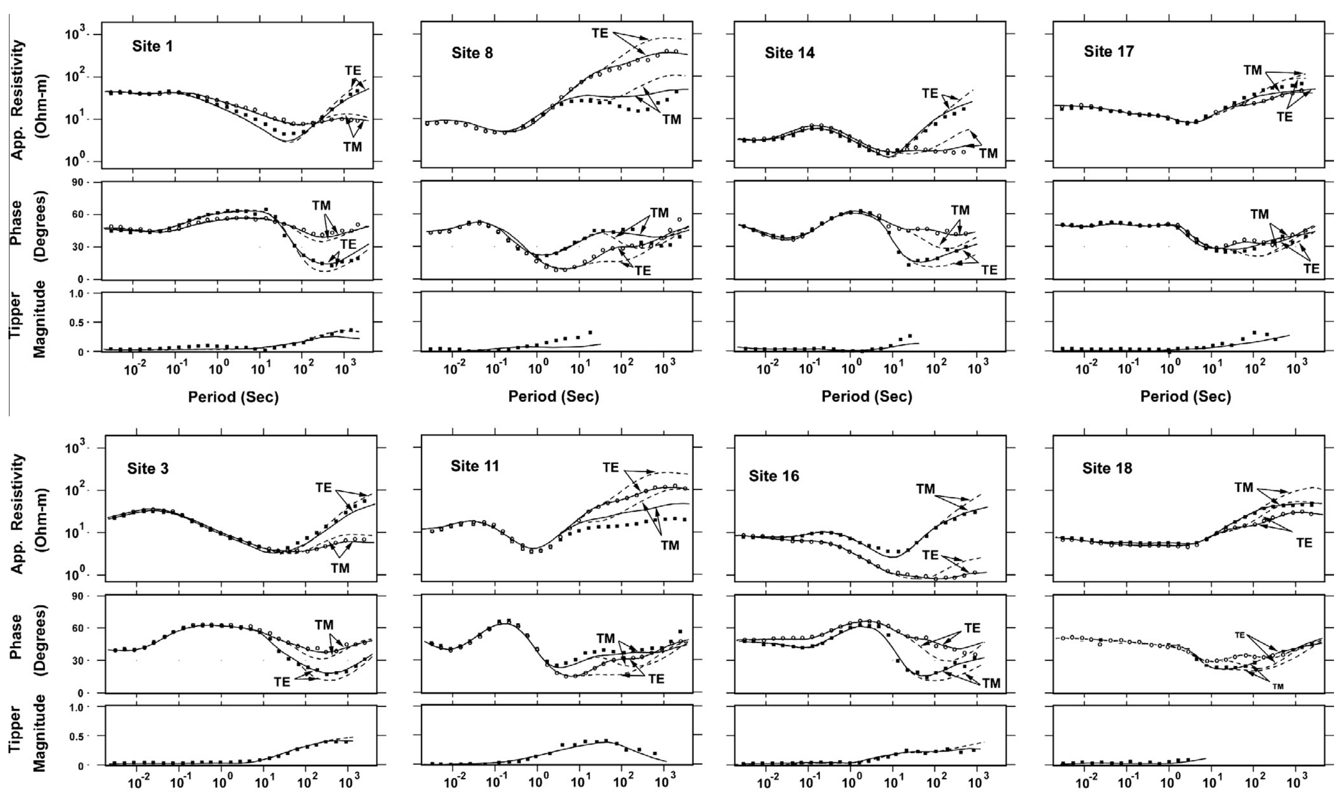

Fig. 12. Results of the tests conducted to determine the sensitivity of the feature (E) in the resistivity section in Fig. 11. The open circles and the filled squares denote the observed data points in TE and TM mode respectively. The solid and hatched lines through the data points are the responses of the model before and after the removal of the low resistivity feature (E) respectively.

values greater than 45 degrees with decreasing frequencies when low resistivity is encountered at deeper levels. Thus these observations provide sufficient evidence for the existence of (E) in Fig. 11.

5. Discussion

The low resistivity layer, A–A′–A at the top is to due to the Irrawaddy sediments which exist over the entire profile except between the sites 7 and 11 where the igneous rocks are present. The large variation of the conductance of this layer (between 20 and 3000 S) is indicative of widely varying environmental conditions during the sedimentation. Since the individual thicknesses and resistivities of low resistivity layers are weakly determined in MT responses, the conductance (thickness conductivity product) of these layers which is a well-determined parameter is referred to in the discussion here. On the basis of the vertical block movements inferred from the isostatic anomalies (Verma et al., 1976) as well as the lateral heterogeneities of the geological structures (Sol et al., 2007) in the Indo Burman and adjoining regions we suggest the possibility of sedimentation in marine environment, which may have caused the high conductance pockets observed here. The seismic studies (Maurin and Rangin, 2009) report the thickness of the Irrawaddy sediments between 10 and 15 km in the central Myanmar basin.

In order to interpret the deep structure more effectively, the Benioff Wadati zone proposed by Ni et al. (1989) is shown in Fig. 11, superimposed over the geoelectric section. It should be noted here that due to the nonavailability of the spatial co-ordinates in the seismic data, the lateral positions is matched using the known position of the exposures of the igneous rocks and hence are subjective to that extent.

The feature (C–C′) with a moderate resistivity of 20–100 Ω m seems to be caused by two inclined faults converging toward each other at depth of 30 km, in close proximity of the low resistivity feature, (E). From the observed correspondence with the Benioff Wadati zone (Ni et al., 1989) the low resistivity (C) seems to be the thrust fault along which the Indian plate (D) and the overlying sediments subduct eastwards beneath the Burmese block (B–B′). The low resistivity (C) may be due to the sediments overlying the subducting Indian plate. The exact surface expression of this subduction zone is not easily decipherable due to the presence of the thick sedimentary overburden and hence no attempt is made to associate this feature with the known faults documented in the geological maps (Fig. 1). Similar low resistivity associations with the subducting plates are observed elsewhere in the Indo Burman range, for example, over the Shillong plateau in the NE India (Gokarn et al., 2008) as well as the Kanchanabur province in Thailand (Boonchaisuk et al., 2013). Normally the deep crustal fluids released during subduction process get trapped causing low resistivities such as the feature (E) at depth of 30 km and beyond. The deep crustal fluids generally comprise the mineralized or saline water or the carbon dioxide (Jones, 1992) rising along the thrust zones from the deeper strata.

In the central part of India, Naganjaneyulu and Santosh (2010) have proposed that the low resistivity zones in the middle crust such as the one observed here may be caused by emplacement of deep mantle material at the brittle ductile zone between the upper and lower crusts in the subduction zones. The similarity of the overall tectonic setting in the present study area with that across the central Indian tectonic zone suggests that similar mafic emplacements could have caused the low resistivity (E) here. However in the absence of additional information from the other geophysical studies, it may be premature to ascertain such a possibility at present.

The causative factors leading to the moderate resistivity (C′) to the east are not immediately apparent. The Sagaing fault is located about 80 km away from the eastern part of the present survey profile and is unlikely to influence the resistivity at (C′). In order to check the seismicity associated with this feature, the earthquake foci recorded between 1890 and 1970 (after Verma et al., 1976) are shown superimposed over the geoelectric section, denoted by open circles in Fig. 11. Some support for a possible fault along C′ is evident from the presence of some earthquake foci over this feature. It seems that another hitherto unknown fault, concealed beneath the thick Irrawaddy sediments may be causing to this low resistivity. As mentioned earlier, the MT studies over the EHS have delineated low resistivity zones in the deep crust (Denghai et al., 2010). The low seismic velocities (Yao et al., 2008) and also the crustal flows near EHS observed from the GPS studies (Gan et al., 2007; Zhang et al., 2004), these low resistivities in the deep crust were attributed to the weakened crust which flows in several channels in clock wise sense around the eastern Himalayan syntaxis. These flows extend to the east up to the Shan plateau. The crustal flows in the channels formed in the weakened crust are also likely to contribute to the low resistivities, (C′) and (E).

The Bouguer gravity along the MT survey profile (top part of Fig. 11) is rather listless, increasing monotonously from a value of −140 mGal to the west to −25 mGal to the east of the MT profile. The thinning of the top sedimentary layer from the west to east, which is broadly reflected in the MT profile as general decrease in the conductance of the top layer may partly explain this decreasing Bouguer gravity. None of the other features in the substructure are reflected in the Bouguer gravity. In the absence of the information on the disposition of the Moho in this region, it is not possible to estimate its contribution to the Bouguer gravity. Generally the Bouguer gravity over subduction zones shows widely differing responses depending upon the velocity as well as the thermal state of the subducting plate (Watts and Talwani, 1975).

6. Conclusions

Magnetotelluric studies over the igneous arc of the Indo Burman Orogen in the Sagaing province have delineated the high resistivity Indian plate (D) at depth of 30 km and beyond subducting beneath the Burmese block, (B–B′). The moderate resistivity of 20–100 Ω m (C) overlying the subducting Indian plate may be due to the Irrawaddy sediments. These results show that the ophiolites on the eastern and western belts do not correspond to the surface expression of the suture as was surmised by Acharya (2007). Both ophiolitic belts seem to exhibit a nappe-like character.

Another deep seated feature (C′) with moderate resistivity (20–100 Ω m) to the east of the Burmese block seems to correspond to a deep seated fault which marks its eastern boundary. This fault is located about 80 km east of the Sagaing fault, which was earlier believed to be the eastern edge of the Burmese block. The nature of the crustal movements over this hitherto unknown fault buried under a thick pile of sediments is not apparent at this stage, although the presence of some earthquake foci over this feature do lend support to the presence of a fault at C′. Sagaing fault seems to be composed of several branches at its northern end as seen in Fig. 1 (Maurin and Rangin, 2009), suggesting that it may be an en echelon fault. Thus the fault proposed in the present work may be a part of Sagaing fault. Alternately, the channel flows in the deep crust beneath the Shan plateau and Sagaing fault observed from the magnetotelluric studies (Denghai et al., 2010), GPS (Gan et al., 2007; Zhang et al., 2004) and the seismic studies (Yao et al., 2008), leading to low resistivity zones in the deep crust may have influenced the deep crustal resistivity in this region.

A deep crustal conductor (E) at depth of 30 km is understood to be caused by the fluids from the deeper levels, normally known to rise along the fractures associated with the subduction zones.

Whereas such fluids at shallow levels escape, those at depth get trapped, thus leading to the low resistivity (E) observed here.

Acknowledgements

The authors express their heart-felt thanks to the Geophysics Group of the NHPC Ltd. for the sponsorship of the project as well as the financial and logistic support provided during the survey and the Myanmar governmental authorities and local authorities in Sagaing province and Monywa for granting the necessary permissions and logistic support. Thanks are also due to the Director, Indian Institute of Geomagnetism for the necessary permissions and approvals. We thank the anonymous reviewer for his critical comments which made significant improvements.

References

Acharya, S.K., 2007. Collisional emplacement history of the Naga-Andaman ophiolites and position of the eastern Indian suture. J. Asian Earth Sci. 29, 229–242.

Acharya, S.K., Mitra, N.D., 1986. Regional geology and tectonic setting of northeast India and adjoining regions: geology of Nagaland Ophiolite. Mem. Geol. Surv. India 119, 6–12.

Bender, F., 1983. Geology of Burma. Gebruder Borntraeger, Berlin.

Boonchaisuk, S., Siripunvaraporn, W., Ogawa, Y., 2013. Evidence for middle Triassic to Miocene dual subduction zones beneath the Shan–Thai terrane, western Thailand from magnetotelluric data. Gondwana Res. 23 (2013), 1607–1616, ISSN 1342-937X, http://dx.doi.org/10.1016/j.gr.2012.08.009.

Curray, J.R., Moore, D.R., Lawver, L.A., Emmel, F.J., Waitt, R.W., Hery, M., Kieckhefer, R., 1979. Tectonics of the Andaman Sea and Burma. In: Watkins, J.S., Montadert, L., Dickerson, P. (Eds.), Geological and Geophysical Investigations of Continental Margins, vol. 29. American Association of Petroleum Geologists Memoirs, pp. 189–198.

Curray, J.R., Emmel, J.F., Moore, D.G., Raitt, R.W., 1982. Structure, tectonics and geological history of the northeastern Indian ocean. In: Nairn, E.M., Stehli, F.G. (Eds.), Ocean basins and margins, vol. 6. Plenum, New York, pp. 399–450.

Denghai, B., Unsworth, M.J., Meju, Max. A., Ma, X., Teng, J., Kong, X., Sun, Y., Sun, J., Wang, L., Jiang, C., Zhao, C., Xiao, P., Liu, M., 2010. Crustal deformation of the eastern Tibetan plateau revealed by magnetotelluric imaging, magnetotelluric studies. Nat. Geosci., http://dx.doi.org/10.1038/NGEO830.

Gan, W., Zhang, P., Shen, Z-K., Niu, Z., Wang, M., Wan, Y., Zhou, D., Cheng, J., 2007. Present-day crustal motion within the Tibetan Plateau inferred from GPS measurements. J. Geophys. Res. 112, B08416, http://dx.doi.org/10.1029/2005JB004120.

Gansser, A., 1980. The peri-India suture zone. In: Aubouin, J., Debelmas, J., Latereille, M. (Eds.), Geology of Alpine Chain Born of Tethys, vol. 115. Bureau de Recherches Géologiques et Mine'res Memoirs, pp. 140–148.

Gokarn, S.G., Gupta, G., Rao, C.K., Selvaraj, C., 2002. Electrical structure across the Indo-Tsangpo suture and the Shyok suture zones in the NW Himalaya using magnetotelluric studies. Geophys. Res. Lett., 29(8)10.1029/2001GL014325, 2002.

Gokarn, S.G., Gupta, G., Walia, D., Sanabam, S.S., Hazarika, N., 2008. Deep geoelectric structure over the Lower Brahmaputra valley and Shillong Plateau, NE India using magnetotellurics. Geophys. J. Int., http://dx.doi.org/10.1111/j.1365-246X.2007.03711.x.

Groom, R., Bailey, R.C., 1989. Decomposition of magnetotelluric tensor in presence of local three dimensional galvanic distortion. J. Geophys. Res. 94, 1913–1925.

Jones, A.G., 1992. Electrical conductivity of the continental lower crust. In: Fountain, D.M., Arculus, R., Key, R.W. (Eds.), Continental Lower Crust. Elsevier, Amsterdam, pp. 81–143.

Jones, A.G., Jodicke, H., 1984. Magnetotelluric transfer function estimation improvement by coherent based technique. In: Paper Presented at 54th Annual International Meeting of Society of Exploration. Geophysics, Atlanta, GA, Dec. 2-6.

Jones, A.G., Chave, A.D., Alud, D., Bahr, K., Egbert, G., 1989. A comparison of techniques for magnetotelluric response function estimation. J. Geophys. Res. 94, 14201–14213.

Kaufman, A.A., Keller, G.V., 1981. Magnetotelluric Sounding Method. Elsevier Scientific Company, Amsterdam, p. 67.

Maurin, T., Rangin, C., 2009. Structure and kinematics of the Indo-Burmese wedge: recent and fast growth of the outer wedge. Tectonics 28, TC2010, http://dx.doi.org/10.1029/2008TC002276.

McNeice, G.W., Jones, A., 2001. Multi site Multi frequency tensor decomposition of magnetotelluric data. Geophysics 66, 158–173.

Mitchell, A.H.G., 1981. Phanerozoic plate boundaries in mainland SE Asia, the Himalaya and Tibet. J. Geol. Soc. Lond. 138, 109–122.

Naganjaneyulu, K., Santosh, M., 2010. The central Indian tectonic zone: a geophysical perspective on continental amalgamation along a Mesoproterozoic suture. Gondwana Res. 18, 547–564. http://dx.doi.org/10.1016/j.gr.2010.2.017.

Ni, J.F., Guzman-Speziale, M., Bevis, M., Holt, W.E., Wallace, T.C., Seager, W.R., 1989. Accretionary tectonics of Burma and the three-dimensional geometry of the Burma subduction zone. Geology 17, 68–71.

Nielsen, C., Chamot-Rooke, N., Rangin, C., ANDAMAN Cruise Team, 2004. From partial to full strain partitioning along the Indo-Burmese hyper-oblique subduction. Mar. Geol. 209, 303–327.

Rodi, W., Mackie, R.L., 2001. Nonlinear conjugate gradients algorithm for 2D magnetotelluric inversions. Geophysics 66, 174–187.

Sol, S., Meitzer, A., Burgmann, R., van der Hilst, R.D., King, R., Chen, Z., Koons, P.O., Lev, E., Liu, Y.P., Zeitler, P.K., Zhang, X., Zhang, J., Zurek, B., 2007. Geodynamics of the southeastern Tibetan plateau from seismic anisotropy and geodesy. Geology 35, 563–566.

Unsworth, M.J., Jones, A.G., Wei, W., Marquis, G., Gokarn, S.G., Spratt, J.E., INDEPTH-MT Team, 2005. Crustal rheology of the Himalaya and Southern Tibet inferred from magnetotelluric data. Nature. http://dx.doi.org/10.2038/nature04154.

Verma, R.K., Mukhopadhyay, M., Ahluwalia, M.S., 1976. Seismicity, gravity and tectonics of the north eastern India and northern Burma. Bull. Seismol. Soc. Am. 66, 1683–1694.

Watts, A.B., Talwani, M., 1975. Gravity effects of down going lithospheric slabs beneath Island Arcs. Geol. Soc. Am. Bull. 86, 1–4. http://dx.doi.org/10.1130/0016-7606(1975) 86<1:GEODLS>2.0.CO;2.

Yao, H., Beghein, C., van der Hilst, R., 2008. Surface wave array tomography in SE Tibet from ambient seismic noise and two-station analysis_II; Crustal and upper-mantle structure. Geophys. J. Int. 173, 205–219.

Zhang, P., Shen, Z., Wang, M., Gan, W., Bürgmann, R., Molnar, P., Wang, Q., Niu, Z., Sun, J., Wu, J., Hanrong, S., Xinzhao, Y., 2004. Continuous deformation of the Tibetan plateau from global positioning system data. Geology 32, 809–812.